

A mathematical model for diffusion with induced crystallization: 2.

Christopher J. Durning* and William B. Russel

Textile Research Institute, and Department of Chemical Engineering, Princeton University, Princeton, New Jersey 08544, USA

(Received 31 October 1983; revised 16 February 1984)

This article extends the analysis of a mathematical model for solvent induced crystallization. By evaluating the model's parameters for polymer/penetrant systems studied previously we find the predicted behaviours to be consistent with those determined experimentally. Fitting a limiting solution to solvent transport data in poly(ethylene terephthalate) films gives the threshold concentrations for crystallization and the penetrant diffusivity in the amorphous component of the highly swollen polymer. Numerical solutions determine the model's behaviour in intermediate regions where analytical solutions do not apply. These predict negative curvature in plots of weight gain *versus* \sqrt{t} and a distinct crystallization front behind a swelling boundary; the former results from the rapid crystallization of swollen surface layers, while the latter indicates partial decoupling between solvent transport and polymer crystallization. We also analyse briefly the desorption process following solvent induced crystallization; the relative magnitude of initial sorption and desorption rates depends on the induced crystallinity and the crystallization rate.

(Keywords: macrovoids; cavitation; solvent induced crystallization; anomalous diffusion; non-Fickian diffusion)

INTRODUCTION

A model proposed for diffusion with induced crystallization combines phenomenological descriptions of the component processes: anomalous diffusion, local crystallization, and macrovoid development (i.e. cavitation). The description incorporates a threshold concentration for crystallization and a sharp boundary, separating swollen from unswollen polymer, which penetrates the sample during sorption. Asymptotic analysis yields two useful, limiting solutions, one for thick films with rapid crystallization, and the other for thin films with slow crystallization (called cases A and B¹, respectively). The asymptotic predictions of transport kinetics, crystallization kinetics and macrovoid patterns resemble the experimental findings for several polymer/penetrant systems. For example, thick PET films with several organic solvents²⁻⁴ apparently obey case A predictions, while thin polycarbonate (PC) films in chloroform⁵ or acetone⁶ exhibit case B behaviour. In this article we verify these connections by evaluating the model's parameters and comparing with the criteria defining the limiting regimes.

Although the limits explain several features of diffusion with induced crystallization, they cannot account for some unusual kinetic behaviour, such as the negative curvature in plots of weight gain *versus* \sqrt{t} ^{2,7-9}, sorption overshoots^{7,9}, and distinct crystallization 'fronts' lagging the solvent front during sorption^{6,10}. To improve the understanding of these we analyse through numerical simulations the behaviour of the model in the intermediate region between the limiting cases.

We also discuss briefly desorption following diffusion

with induced crystallization, since neither a mathematical nor experimental analysis of this process has appeared in the literature.

MATHEMATICAL MODEL

From the previous development¹, the following dimensionless equations describe diffusion in one direction with simultaneous crystallization:

solvent mass balance in partially swollen region, ($\lambda_s \leq \xi < \lambda$)

$$\frac{\partial}{\partial \xi} (1-f) \frac{\partial \gamma}{\partial \xi} = \frac{\partial}{\partial \tau} (1-f) (\gamma + q) \quad (A)$$

$$\gamma = 1 \text{ for } \tau = 0, \xi = 0 \quad (B)$$

$$\gamma = 1 \text{ for } \tau > 0, \xi = \lambda_s \quad (C)$$

$$-\frac{\partial \gamma}{\partial \xi} = \begin{cases} (\gamma + q) \frac{d\lambda}{d\tau} & \text{for } \tau < \tau_p, \xi = \lambda \\ 0 & \text{for } \tau \geq \tau_p, \xi = \lambda_p \end{cases} \quad (D) \quad (D')$$

Kinetics at swelling boundary, ($\xi = \lambda$)

$$\frac{d\lambda}{d\tau} = \gamma^n \quad (E) \quad (1)$$

$$\lambda = 0 \text{ for } \tau = 0$$

crystallization in saturated and partially swollen regions, ($0 \leq \xi < \lambda$)

$$\frac{\partial f}{\partial \tau} = \Omega h(\gamma) f^{2/3} (f_0 - f) \quad (F)$$

$$f = f_1 \text{ for } \tau = 0$$

* Current address: Department of Chemical Engineering and Applied Chemistry, Columbia University, New York 10027, USA

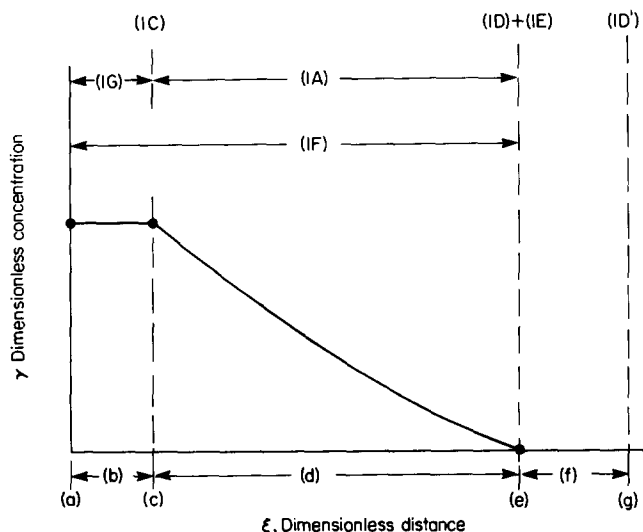


Figure 1 Hypothetical, dimensionless concentration profile for the transport process described by equations (1). Distinct regions are labelled in the lower half; the domain of each relationship appears in the upper half. Key: (a) = film surface, (b) = saturated region, (c) = saturation boundary ($\xi = \lambda_s$), (d) = partially swollen region, (e) = swelling boundary ($\xi = \lambda$), (f) = glassy region, (g) = film centerline ($\xi = \lambda_p$)

macrovoid formation in saturated regions, ($0 \leq \xi < \lambda_s$)

$$\begin{aligned} \gamma &= 1 \\ \varepsilon &= \frac{v_1^0}{(1-v_1^0)} [f-f^*] \quad (G) \\ \lambda_s &= 0 \text{ for } \tau = 0 \end{aligned}$$

Figure 1 shows a hypothetical, dimensionless concentration profile for the transport process described in Ref. 1, and indicates the domain of each relationship.

The dimensionless variables γ (concentration), f (crystallinity), ε (void fraction), λ (penetration depth of the swelling boundary), τ (time) and ξ (distance into the sample) have been defined previously¹. q is the dimensionless threshold concentration for swelling and n is an empirically determined exponent in the expression for swelling kinetics. $\lambda_p = \Lambda_p U_0 / D$ represents the dimensionless film half depth, while $\tau_p = t_p U_0 / D$ represents the dimensionless time required for complete penetration of the film by the swelling boundary (i.e. for $\lambda = \lambda_p$). Here, Λ_p is half the film thickness, t_p the time for complete penetration, U_0 the initial velocity of the swelling boundary, and D the penetrant's diffusivity (polymer fixed frame) in the amorphous component of the swollen polymer. Ω represents the dimensionless crystallization rate:

$$\Omega = \frac{D}{U_0^2} \left(36\pi N_s / V_E \right)^{1/3} \frac{G_0}{f_0} S = \frac{\text{time scale for transport}}{\text{time scale for crystallization}}$$

where N_s / V_E is the nucleation density, G_0 a pre-exponential factor in the expression for the crystallite growth rate G , S a scaling factor given by the maximum value of G/G_0 , and f_0 the ultimate crystallinity.

The first of equations (1) describes unsteady diffusion of penetrant in the partially swollen, crystallizing polymer behind the swelling boundary. The next three equations, (1B-D) are the initial and boundary conditions for

sorption in an initially dry film. The moving boundary condition, (1D), couples with a semi-empirical rate expression, (1E), for the swelling process localized at the boundary λ . It becomes a no flux condition, (1D'), when the film is penetrated completely by λ (i.e. for $\tau \geq \tau_p$).

The crystallization equation, (1F), determines the local crystalline volume fraction, f , within the partially swollen and saturated regions. $h(\gamma) = G/G_0 S$, is an O(1) function accounting for the concentration dependence of the crystallite growth rate. The relationships (1G) define an embedded moving boundary problem for the location of saturated regions, delimited by a saturation boundary, λ_s . Here, phase separation occurs, producing pockets of pure liquid solvent which leave macrovoids in the dried sample. f^* represents the local crystalline volume fraction when saturation first occurs.

As mentioned, useful analytical solutions to (1) are possible for thick films with rapid crystallization, and for thin films with slow crystallization; the asymptotic behaviours are summarized in *Table 1*.

The conditions necessary for case A behaviour are:

$$\tau_p \gg 4M^2 e^{2M^2} \left\{ \frac{(1-v_1^0)(1-f_0)}{(1-v_1^0-f_0)} \frac{Q}{1+q} \right\}^2; \quad \tau_p \gg 1/4M^2 \Omega \quad (2)$$

while those necessary for case B are:

$$\tau_p \ll 4m^2 e^{2m^2} \left(\frac{q}{1+q} \right)^2; \quad \tau_p \ll 1/\Omega \quad (3)$$

Here, v_1^0 is the solvent volume fraction in the amorphous component of the polymer at saturation, while m , M and Q are constants related to q and f_0 .

PUBLISHED EXPERIMENTAL DATA

Table 2 summarizes selected experimental results found by previous workers for poly(ethylene terephthalate) (PET), polycarbonate (PC), and isotactic polystyrene (IPS) systems. *Figure 2* illustrates three transport effects of interest with experimental data from Makarewicz¹¹, Ware *et al.*⁷ and Overbergh *et al.*⁹, corresponding to No. 5 and 14-17 in *Table 2*. (The smooth curves in *Figure 2* were drawn by the original authors as empirical representations of their data.) The interesting effects follow:

Table 1 Summary of asymptotic behaviours

Case	Description	Transport behaviour	Crystallization behaviour	Macrovoid patterns
A	Thick films, rapid crystallization	Solvent diffusion controlled, weight gain increases linearly with $\sqrt{\tau}$	Solvent diffusion controlled, crystallinity increases linearly with $\sqrt{\tau}$	Surface macrovoids only
B	Thin films, slow crystallization	Polymer swelling controlled, weight gain increases linearly with t	Polymer crystallite growth controlled, Avrami kinetics	Macrovoids distributed uniformly throughout

Table 2 Summary of published experimental behaviour

No.	Ref.	Liquid	Temperature (°C)	Film half depth (cm)	Reported experimental behaviour (see key)
<i>Poly(ethylene terephthalate) (PET)</i>					
1	4	Methylene chloride	25	0.121	a
2	2,3,11	Methylene chloride	24	0.125	a, b, c, g
3	4	Methylene chloride	26	0.0146	g
4	4	1,4 dioxane	25	0.121	a
5	2,3,11	1,4 dioxane	24	0.125	a, b, c, g
6	4	1,4 dioxane	25–100	0.0146	e, g
7	2,3,11	Nitromethane	24	0.125	a, b, c, g
8	4	Nitromethane	0–50	0.0146	e
9	2,3,11	Acetone	24	0.125	a, b, c, g
10	12	Acetone	25	0.0010	h
<i>Polycarbonate (PC)</i>					
11	8	Acetone	25	0.178	a, c, g
12	6	Acetone	20–48	0.005	f
13	6	Acetone	20–48	0.001	f
14	7	Acetone	25	0.332	b, c
15	7	Acetone	25	0.015	f
<i>Isotactic polystyrene (IPS)</i>					
16	9	Methylene* chloride	30	0.100	c, d
17	9	Methylene* chloride	30	0.0125	d, f

* Methylene chloride vapour at 85% activity

Key for experimental behaviour

Transport behaviour

- a — solvent diffusion controlled penetration kinetics; penetration depth Λ increases linearly with \sqrt{t} .
- b — solvent diffusion controlled weight gain; weight gain increase linearly with \sqrt{t} .
- c — weight gain versus \sqrt{t} plot exhibits negative curvature.
- d — polymer swelling controlled weight gain; weight gain increases faster than linear with \sqrt{t} .

Crystallization behaviour

- e — solvent diffusion controlled crystallization kinetics; overall crystallinity increases linearly with \sqrt{t} .
- f — evidence for decoupling between solvent transport and crystallization (Avrami kinetics, distinct crystallization front, or sorption overshoot); crystallite growth control of crystallization kinetics.

Macrovoid patterns

- g — surface macrovoids.
- h — evidence for internal voids (density, small-angle X-ray scattering, electron microscopy).

† Experimental behaviour is reviewed in more detail in Ref. 1

(1) For relatively thick films, plots of weight gain versus \sqrt{t} exhibit negative curvature before approaching diffusion controlled behaviour (i.e. linear with \sqrt{t}).

(2) For intermediate thicknesses, and for thin films, the weight gain plots exhibit positive curvature initially, that is, they increase faster than linear with \sqrt{t} .

(3) For relatively thin films, sorption overshoots (i.e. peaked maxima) occur.

The first effect, indicated in Figure 2a and b, cannot be explained by existing theories for non-Fickian diffusion^{13–16}. Wilkes *et al.*^{2,4} attributed this peculiar sorption behaviour to the formation of surface macrovoids, which was thought to increase temporarily the effective surface area for sorption.

Effect (2), appearing in Figure 2c, suggests that swelling controlled transport (i.e. Case II diffusion) occurs initially by analogy with the sorption behaviour in non-crystallizable glassy polymers¹⁶. Interestingly, for the thicker IPS specimen in Figure 2c, (2) and (1) occur sequentially (a comparison with the sorption data for an atactic polystyrene sheet with the same thickness clearly shows that effect (1) is present towards the end of sorption). One might speculate that (2) and (1) generally appear sequentially, but that the relative prominence of

each depends on the polymer/penetrant system and the experimental conditions.

Figures 2b and c illustrate effect (3). Previous workers^{5–7,9} attributed sorption overshoots to substantial crystallization occurring after sorption is complete; apparently, solvent occluded from developing crystallites desorbs from the fully swollen specimen to produce an overshoot. In Table 2, we regard overshoots as evidence for decoupling between the solvent transport and polymer crystallization processes.

CLASSIFYING THE EXPERIMENTAL DATA

Independent knowledge of the physical properties for the systems listed in Table 2 allows the estimation of the parameters in the model and quantitative evaluation of the criteria for limiting behaviours. Hence, we can classify these systems as limiting cases or as intermediate between the asymptotes. The required transport properties and crystallization rate constants are available or can be estimated (Table 3); however, no data are available for the parameter q . Here we adopt 1/2 as a representative value, and later demonstrate its validity for PET systems. A typical value¹⁷ of 0.30 is assigned to both f_0 and v_1^0 .

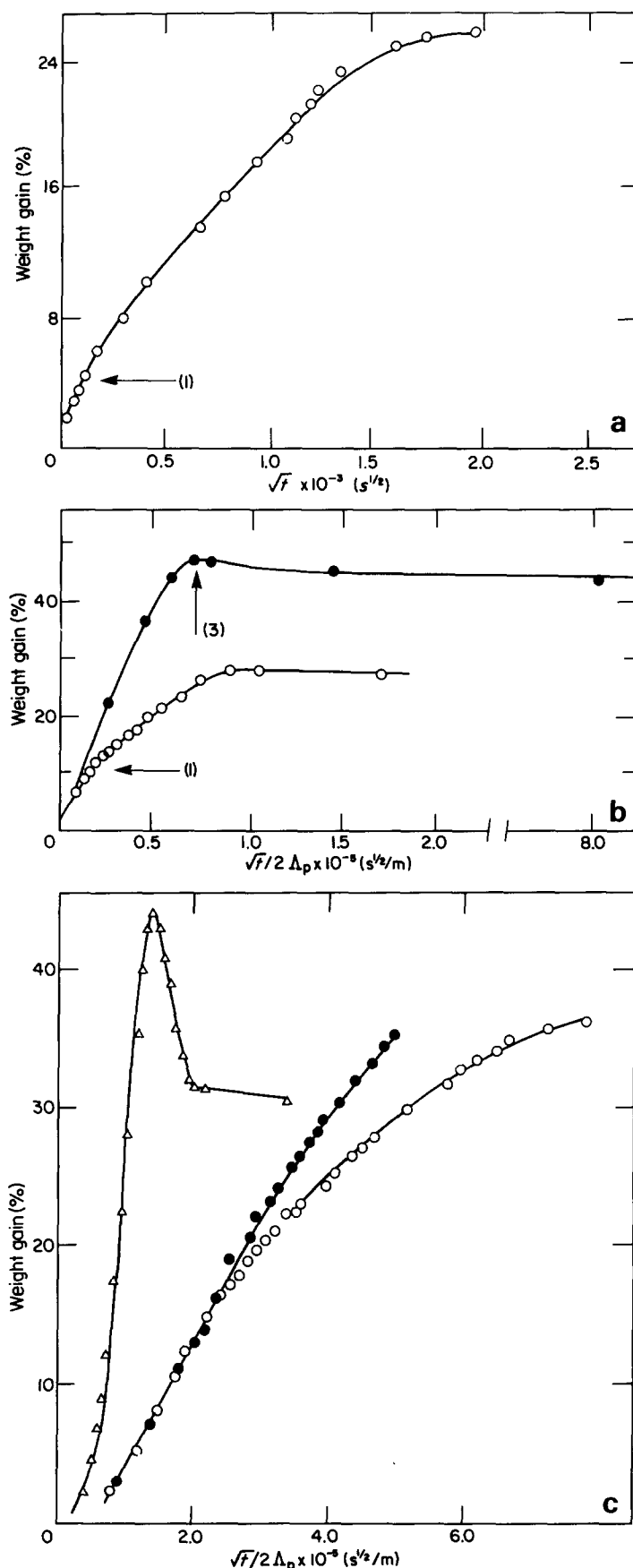


Figure 2 Transport data for diffusion with induced crystallization: (a) weight gain and penetration depth versus \sqrt{t} for 1,4-dioxane in 0.25 cm thick PET films at 24°C (Makarewicz¹¹), (b) weight gain versus $\sqrt{t/2A_p}$ for acetone in PC films at 25°C, $2A_p=0.03$ cm (●), 0.162 cm (○) (Ware *et al.*⁷), (c) weight gain versus $\sqrt{t/2A_p}$ for methylene chloride in IPS at 30°C, $2A_p=0.02$ cm (○), 0.025 cm (△), 0.2 cm atactic polystyrene (●) (Overbergh *et al.*⁹)

We estimated the initial penetration velocity, U_0 , from the data points appearing in the pertinent references. In the absence of moving boundary data for IPS systems, we used the upper bound of U_0 for hydrocarbons in atactic polystyrene¹⁸. The values of the diffusion coefficient were estimated from diffusion controlled penetration depth data using the formula suggested by Turska⁶. This gives the quantity $2M^2D$ by comparing with the diffusion controlled limit of our theory; subsequent calculations for PET systems demonstrate that $2M^2 \sim O(1)$. For IPS systems, the integral value of the diffusivity at 85% solvent activity⁹ was used. We have ignored the small variations in temperature ($\sim \pm 5^\circ\text{C}$) when applying these to the systems in Table 2.

Ultimate crystallinities for most systems have been compiled previously¹⁷; that for PET in 1,4 dioxane was measured by density¹⁹, while that for IPS was determined calorimetrically⁹. The nucleation density in PET is that determined by Makarewicz³ for melt cast films without additives. For PC and IPS the values were calculated from the reported average spherulite sizes^{8,9}. G_0 was taken from Makarewicz³ for PET, from Boon and Azcue²⁰ for IPS, and was estimated from the value of G for the pure polymer at 195°C²¹ in the case of PC. We have ignored possible differences in molecular weight when using these values of G_0 for the systems in Table 2. The Appendix summarizes the calculation of S , a scaling factor for the function $h(\gamma)$.

Table 4 lists the values of Ω computed to one significant figure from the data in Table 3. Except for 1,4 dioxane in PET, the values in PET and IPS systems are $\sim O(10-10^2)$, while that for acetone in PC is $\sim O(1)$. We feel the estimate for 1,4 dioxane/PET is spuriously low. Ω depends on the glass transition temperature (T_g) of the polymer/penetrant system, which we estimated assuming free volume additivity of the components. This requires T_g for the solvent (see Appendix), taken as 50°C below the liquid's melting point⁷. The symmetrical molecule, 1,4 dioxane, has a rather high melting point relative to the other solvents considered, giving a large value of T_g and a small value of Ω . Using the T_g for dioxane recommended by Makarewicz³ gives a very large value of Ω (~ 300). The actual value probably lies near the results for methylene chloride, acetone and nitromethane in PET.

Table 5 lists λ_p to one significant figure for the systems in Table 2 together with the behaviour expected from the criteria for the limiting regimes. If the inequalities defining the limits were fulfilled by less than an order of magnitude the questionable parameter appears in parentheses. Systems not satisfying any of the criteria are considered intermediate. The predictions for dioxane/PET assume $\Omega \sim O(10)$.

Consistency of the observed and expected behaviours

We now discuss the consistency of the observations listed in Table 2 with the expectations from Table 5. Ten of the seventeen conditions listed in Table 5 are classified as thick films with rapid crystallization (case A). Comparing their reported behaviours with those predicted for case A in Table 1 shows substantial agreement. Two discrepancies require explanation, however: one case (No. 16) shows swelling controlled transport initially, and several cases (Nos. 2, 5, 7, 9, 11, 14) exhibit negative curvature in plots of weight gain versus \sqrt{t} . The former system has a marginal value of λ_p (Table 5) and may actually cor-

Table 3 Physical data for evaluating the limiting criteria

(a) Transport data

Polymer	Penetrant	Temperature (°C)	U_0 (cm s ⁻¹ × 10 ⁶)	D (cm ² s ⁻¹ × 10 ⁶)	Ref.
PET	Methylene chloride	24	80	51.1	2
	1,4 dioxane	24	3	0.46	2
	Nitromethane	24	4	2.09	2
	Acetone	20	5	0.67	2
PC	Acetone	20	160	74.6	6
IPS	Methylene* chloride	25	10†	24.7	9

* Penetrant at 85% activity

† Upper bound value for hydrocarbons in atactic polystyrene¹⁸

(b) Crystallographic data

Polymer	Penetrant	Ultimate crystallinity (f_0)	Nucleation density (nm ⁻³ × 10 ¹⁰)	G_0 (nm s ⁻¹ × 10 ⁻⁷)	S (× 10 ⁶)
PET	Methylene chloride	0.424	5.12	3.4	1.3
	1,4 dioxane	0.44	5.12	3.4	0.00092
	Nitromethane	0.492	5.12	3.4	0.043
	Acetone	0.583	5.12	3.4	1.3
PC	Acetone	0.20	5800	1.5 × 10 ⁵	3.7 × 10 ⁻⁵
IPS	Methylene chloride	0.23	460	15	0.019

Sources of data of methods of calculation are given in the text

Table 4 Estimates of Ω (20°–25°C)

Polymer	Penetrant	Ω
PET	Acetone	80
	Dethylene chloride	30
	Nitromethane	20
	1,4 dioxane	0.2 (300*)
IPS	Methylene chloride	30
PC	Acetone	3

* Calculated using 100K for T_g of dioxane³

respond to intermediate conditions since the λ_p values are only approximate. In the latter cases, the weight gain plots show negative curvature only during the initial stages of sorption, the remaining portions of the plots being linear as in *Figures 2a* and *b*. The numerical calculations presented later predict exactly this effect for thick films; the asymptotic solutions cannot since one must linearize the model for their derivation¹.

Nevertheless, the thick film asymptotic solutions represent the experimental behaviour for case A systems reasonably well. To demonstrate this, the weight gain data for Nos. 2, 5, 7 and 9 in *Table 2* have been fitted with the appropriate analytical solution¹

$$W(t) = 2Me^{M^2c^*}\sqrt{Dt} \quad \text{for } t \leq t_p$$

$$W(t)/W(\infty) = 1 - \frac{2}{(1+Q)\text{erf}M} \sum_{n=0}^{\infty} A_n e^{-(k_n/\Lambda_p)^2 D(t-t_p)} \quad \text{for } t > t_p$$

which is written in dimensional form. Here, c^* means the threshold concentration on the rubber side of the swelling boundary and $W(\infty)$ the ultimate weight gain. M , Q , k_n and A_n are constants determined by c^* , c_0 and f_0 . c_0 , the penetrant's solubility in the amorphous polymer, and f_0 , the ultimate crystallinity, have been determined experimentally. c^* , the threshold concentration, and D , the diffusivity, were treated as adjustable constants. Half the swollen film thickness was used for Λ_p .

Figure 3 illustrates the agreement between the asymptotic theory and experiments with methylene chloride in PET (No. 2 in *Table 2*). Since the model was fitted to the weight gain data, the precise agreement of the penetration depth data with the prediction shows the model to be self consistent.

Table 4 shows the constants computed by this procedure. The diffusion coefficients exceed those calculated by Makarewicz² from Fick's law by an order of magnitude. Also, the computed values of q support the earlier presumption of 1/2 as a typical value for evaluation of the limiting criteria.

Values of \bar{c}^*/c_0 obtained from free volume relationships¹⁷ enable the calculation of c^*/\bar{c}^* . Since \bar{c}^* represents the threshold concentration on the glassy side of the swelling boundary, c^*/\bar{c}^* gives the partition ratio for the solvent across the swelling boundary.

According to the theory, only one system in *Table 5* (No. 13) should exhibit case B behaviour. In this case, Turska *et al.*⁶ found that sorption completely terminates before crystallization begins. Using a light transmission technique, they measured the crystallization kinetics, and found sigmoidal curves characteristic of polymer crystallization without solvent transport limitations (i.e. Avrami type kinetics²²); evidently, complete decoupling between solvent transport and polymer crystallization occurs. This behaviour corresponds exactly to that predicted by the case B asymptotic limit.

The intermediate systems in *Table 5*, and the one marginal case (No. 16), display behaviour which clearly lies between the predictions for thick and thin films. For example, in No. 16 (0.2 cm thick IPS films exposed to methylene chloride) the weight gain initially increases faster than linear with \sqrt{t} , as predicted for thin films, but also shows the negative curvature found during the initial weight gain in thick films. Similarly, the distinct crystallization fronts observed lagging the solvent front in No. 12, and the sorption overshoots recorded in Nos. 12, 13, 15 and 17, suggest partial decoupling between solvent transport and crystallization. Evidence for internal voids also

Table 5 Expected behaviour for the systems in Table 2

Polymer	Penetrant	# in Table 2	$\lambda\rho$	Expected behaviour*
PET	Methylene chloride	1	20	A
	Methylene chloride	2	20	A
	Methylene chloride	3	2	intermediate
	Dioxane	4	80	A
	Dioxane	5	80	A
	Dioxane	6	8	A
	Nitromethane	7	30	A
	Nitromethane	8	3	intermediate
	Acetone	9	90	A
	Acetone	10	0.7	intermediate
PC	Acetone	11	40	A
	Acetone	12	1	intermediate
	Acetone	13	0.2	B
	Acetone	14	70	A
IPS	Acetone	15	3	intermediate
	Methylene chloride	16	4	A ($\lambda\rho$)
	Methylene chloride	17	0.5	intermediate

* See Table 1

Table 6 Fit of weight gain data in PET films^{2,11} with Case A equations

Penetrant	#	D ($\text{cm}^2 \text{ s}^{-1} \times 10^8$)	M	Q	q	c^*/c_0	c^*/\bar{c}^*
Methylene chloride	2	130	0.39	3.0	0.74	0.42	5.2
1,4 dioxane	5	4.3	0.28	6.0	0.92	0.48	8.4
Nitromethane	7	3.6	0.36	3.6	0.66	0.40	2.1
Acetone	9	6.1	0.22	10.0	0.61	0.38	4.0

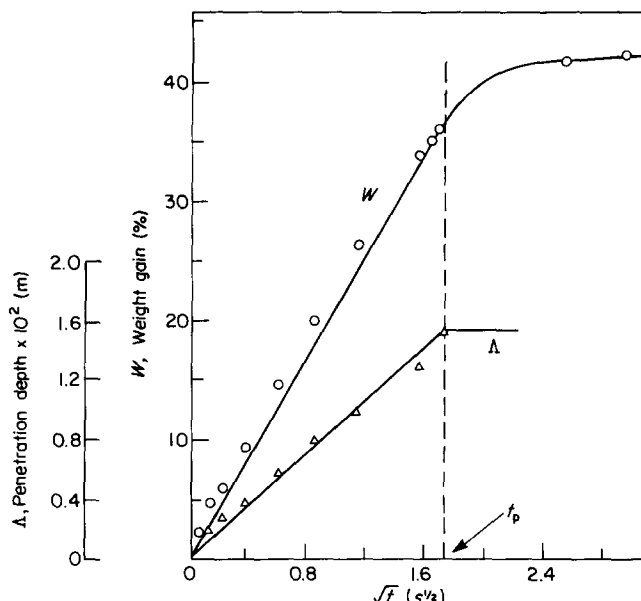


Figure 3 Fit of thick film asymptotic solution (case A) to experimental weight gain and penetration depth data for methylene chloride in 0.25 cm thick PET film at 24°C. Data taken from Makarewicz¹¹

appears in the intermediate region in No. 10. To determine more precisely the model predictions in the intermediate cases, (1) must be solved numerically.

NUMERICAL SOLUTIONS

Our finite difference solution to (1) uses the 'fully implicit' difference scheme²³ for the diffusion equation, which combines backward and central differences for the time and space derivatives, respectively. Simple forward differ-

ences are used for the swelling and crystallinity equations (1E and 1F). Because of the moving boundary, λ , each time step, $\Delta\tau$, adds a grid point to the domain of (1A). During the calculations, we adjust $\Delta\tau$ to move λ a constant step length, h , using equation (1E), providing equally spaced grid points for solving the diffusion equation.

An iterative calculation handles the nonlinearity in the moving boundary condition, (1D), and an updating procedure minimizes the accumulated error from the approximations in solving the nonlinear diffusion equation. A searching routine locates saturated regions after each time step, and calculates the local void fraction using (1G). Figure 4 summarizes the algorithm.

A rigorous proof of convergence is not possible for this problem, but the consistency of the numerical and limiting analytical solutions¹ supports the former's validity. Additional support comes from the calculations with $\Omega=f_1=0$; our results agree with Astarita's for the problem without crystallization solved by an explicit finite difference method. Finally, the results calculated with moderate time steps ($=10^{-2}$) and with small time steps ($=10^{-4}$) agree closely, consistent with convergence.

Subsequently, we investigate the effect of the crystallization rate, Ω , and the ultimate crystallinity, f_0 , on the transport and crystallization kinetics, and give mechanistic interpretations of the predicted effects. The influence of the parameters n and q is not discussed since Astarita *et al.*¹⁶ thoroughly investigated these for the analogous problem in non-crystallizable, glassy polymers. Realistic values²³ of $n=2$ and $q=1.5$ are used throughout (selecting $q=1.5$ as typical rather than 0.5 used in the previous section, is based on a more involved analysis of recently measured sorption data for PET systems²⁵). Also, we evaluated $h(\gamma)$ for methylene chloride in PET at room temperature (22°C), which typifies most interactive poly-

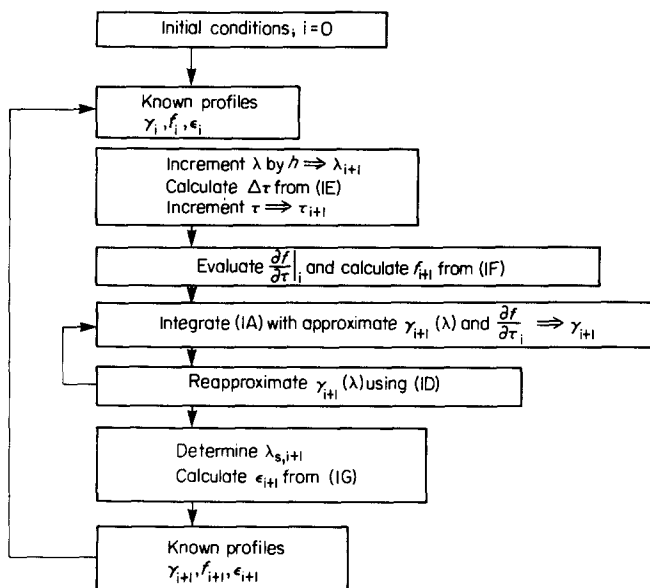


Figure 4 Procedure for numerical solution of mathematical model. The index i refers to time

Table 7 Effect on the penetration time of the crystallization conditions

Crystallization rate	Ultimate crystallinity	τ_p for $\lambda_p = 0.80$
1.0	0.40	1.903
10.0	0.40	1.869
100.0	0.40	1.921
10.0	0.10	1.908
10.0	0.65	1.802

mer/diluent pairs. The specific nature of the diluent affects primarily the magnitude of the scaling factor, $S(T)$, and the 'window' of accessible concentrations (i.e. $c^* < c < c_0$), without grossly altering the behaviour of $h(\gamma)$.

Although the calculations assume semi-infinite slabs, the results pertain also to finite films before complete penetration by the swelling boundary¹. The results are presented for time scales corresponding to film penetration times spanning the intermediate region.

NUMERICAL RESULTS

Table 7 shows the effect on the penetration time of an intermediate film ($\lambda_p=0.8$) of altering substantially the crystallization rate and the ultimate crystallinity. The calculations employ $f_1=0.05$. The results indicate a weak minimum in the time needed to penetrate the film as a function of Ω , illustrating the two opposing influences which crystallization has on the transport kinetics. On the one hand, it may promote penetration by supplying solvent occluded from crystallites to the moving front; on the other, the blocking effect of crystallites tends to curtail penetration. The latter effect apparently dominates when increasing f_0 at constant Ω .

Integration of the transient concentration profiles over the penetrated portion of the film determines the weight gain kinetics. Figure 5 shows the weight gain plotted against the square root of time for several values of Ω at $f_0=0.40$. In general, the initial stages of transport show

case II characteristics; the weight gain increases linearly with time. Apparently Fickian behaviour follows shortly thereafter. The blocking effect of crystallites is evident from the faster weight gain at low rates of crystallization. For $\Omega=10$ very slight negative curvature appears in the weight gain plot, flattening the curve and promoting the appearance of Fickian behaviour.

Elevating the ultimate level of crystallinity causes the weight gain curves to deviate more towards the abscissa before becoming linear with \sqrt{t} (Figure 6). The negative curvature predicted for $f_0 \approx 0.5-0.6$ is about the same as that observed initially in thick films. For thick films, i.e. for large λ_p , the numerical calculations predict negative curvature confined to the initial stages of sorption, with the weight gain increasing linearly with \sqrt{t} thereafter. Extrapolation of the linear portion to the ordinate gives a positive intercept, as illustrated in Figure 6. These predictions mimic the experimental curves for thick films (c.f. Figures 2 and 6) except for the very early stages of sorption

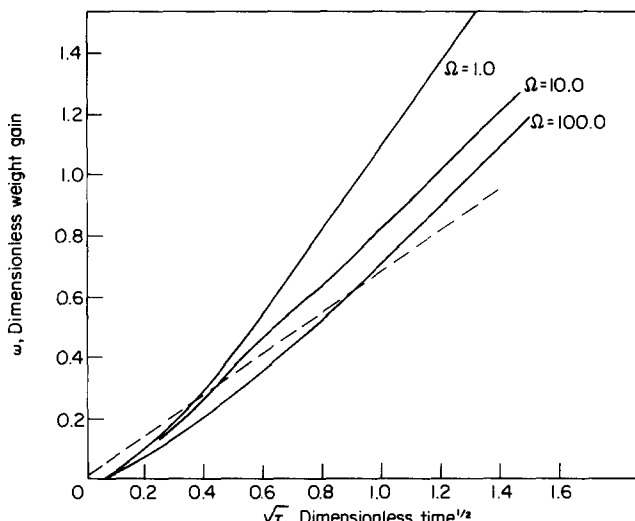


Figure 5 Predicted weight gain (loss) kinetics showing the effect of the crystallization rate, Ω . The dashed line shows the initial desorption rate. The model parameters are given in the text

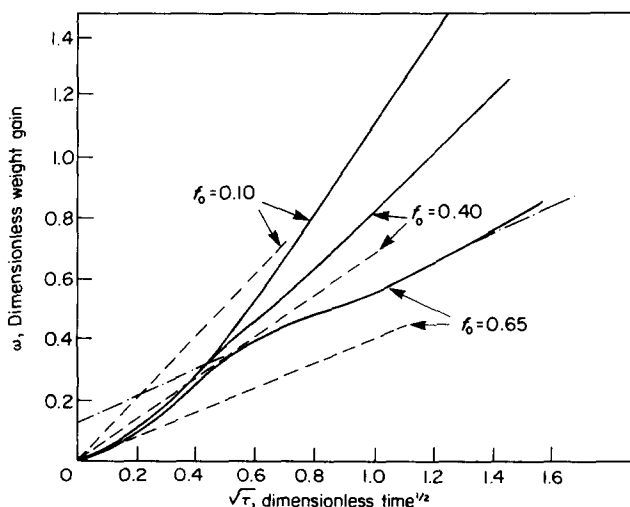


Figure 6 Predicted weight gain (loss) kinetics showing the effect of the ultimate crystallinity, f_0 . (—) shows an extrapolation from an apparently linear portion of the plot. (---) show the initial desorption rates. The model parameters are given in the text

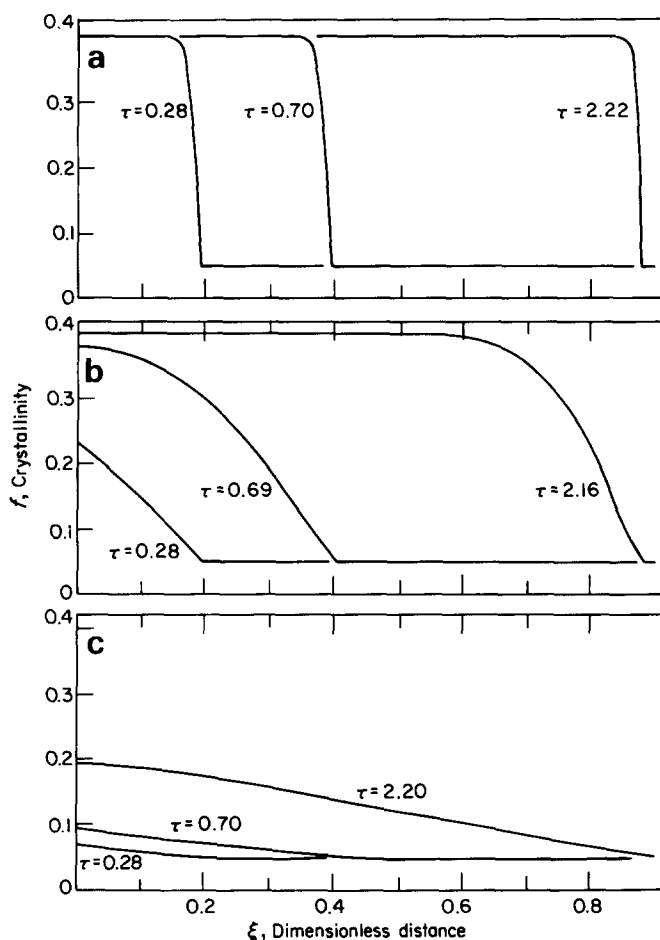


Figure 7 Crystallinity profiles at moderate characteristic times showing the effect of the crystallization rate, Ω . (a) $\Omega=100$, (b) $\Omega=10$, (c) $\Omega=1$. Ultimate crystallinity, f_0 , is 0.40; the remaining model parameters are given in the text

where upward curvature is predicted, but cannot be observed.

The predictions of negative curvature in the weight gain *versus* \sqrt{t} plots clarify the underlying mechanism. Rapid, swelling controlled uptake occurs initially in the amorphous surface layers. Rapid crystallization near the surface follows, supplementing the surface flux with the penetrant occluded from crystallites, and producing macropores via phase separation. With continued penetration, and with the tortuosity introduced by developing crystallites, additional uptake encounters increasing diffusional resistance leading to apparently Fickian behaviour.

For films having intermediate values of τ_p , the model's predictions are qualitatively correct. For example, the weight gain plot predicted for $f_0 = 0.65$, $\Omega = 10$ and $\tau_p = 1$ (Figure 6) resembles the weight gain of methylene chloride in 0.2 cm thick IPS films (Figure 2c). The present calculations do not reproduce the sorption overshoots seen in PC and IPS systems, however; these are discussed in greater detail elsewhere^{24,25}.

Figure 7 shows transient crystallinity profiles developing behind the swelling boundary for different values of the crystallization rate. For high rates the profiles nearly coincide with the solvent front; one could not distinguish a distinct region of amorphous rubber behind the swelling boundary experimentally. At lower rates a crystalline 'front' is predicted, lagging the solvent front, correspond-

ing to the experimental observations in the intermediate system No. 12. For very small values of Ω , crystallization and transport clearly decouple, as in the thin film limit.

In Figure 8, the overall extent of crystallization behind the moving front is plotted as a function of time, displaying the sequential nature of transport and crystallization. An induction time is predicted, shown by the intersection of the extrapolated portion of the plot with the abscissa. For a brief, initial period, little or no crystallization takes place behind the swelling boundary. Clearly, for finite Ω , the initiation of transport delays crystallization to some extent, illustrating the tendency for intermediate systems to show decoupling between the transport and crystallization processes.

KINETICS OF DESORPTION

Fujita¹⁴ points out that, if Fick's second law governs diffusion in a thin slab, the initial rate of sorption always exceeds the initial rate of desorption for diffusion coefficients which increase with concentration as in polymer/diluent systems. Experimental data showing the opposite then indicate non-Fickian diffusion, even if the sorption curves appear to be Fickian. We now compare the sorption and desorption curves when induced crystallization occurs, according to the model.

The expected desorption behaviour for crystallizable glassy polymers is easily extracted from Astarita and Joshi's treatment²⁶ of the problem without crystallization. When the external penetrant activity suddenly drops to zero in the desorption experiment, the surface layers of the fully swollen specimen glassify. During desorption, the thickness of the glassy layer steadily increases, analogous to the swollen layer during sorption. Astarita and Joshi show that, for typical values of the transport parameters and time scales, the thickness of the glassy layer remains negligible throughout desorption. Hence, the diffusional resistance during desorption lies in the bulk of the partially swollen sample; the process proceeds according to Fick's law with a surface con-

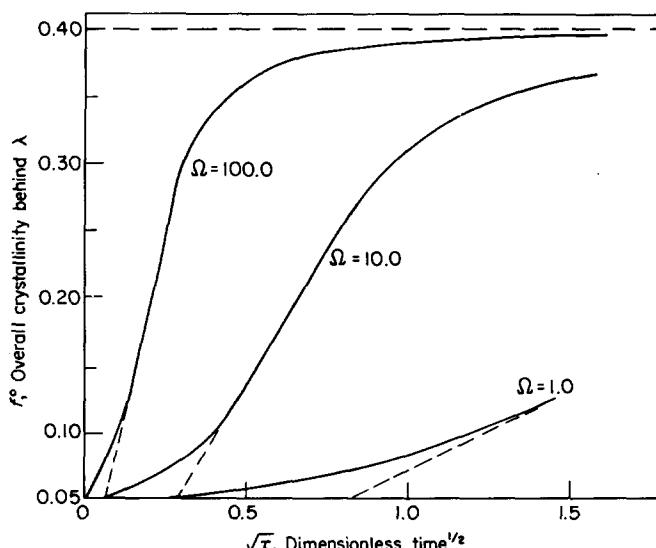


Figure 8 Prediction of overall crystallinity, f_0 , behind the moving boundary as a function of \sqrt{t} , showing the effect of the crystallization rate, Ω . An induction time is shown as the intersection of the dashed line with the abscissa. Model parameters are given in the text

centration of c^* (the value at the glass/rubber interface) and the swollen phase value of the diffusion coefficient. The residual content asymptotes to the threshold value; further desorption requires an inordinately long time, reflecting the extremely small diffusion coefficient in the glassy material.

From this, the solution of the boundary value problem for desorption from the swollen, semi-crystalline polymer gives the initial surface flux:

$$-(1-f_0) \frac{\partial \gamma}{\partial \xi} \Big|_{\xi=\tau=0} = \frac{-(1-f_0)}{\sqrt{\pi t}}$$

resulting in the initial desorption rate:

$$\omega_{\tau=0} = \frac{2(1-f_0)}{\sqrt{\pi}} \sqrt{\tau}$$

plotted as dashed lines in *Figures 5 and 6*. Depending on the crystallization conditions, the initial desorption rate may be greater than or nearly equal to the initial sorption rate. At a given ultimate crystallinity, the sorption curves intersect the desorption line later as Ω increases (*Figure 5*), reflecting the increased resistance to sorption from more rapidly developing crystallites. Increasing the ultimate crystallinity for a given crystallization rate (*Figure 6*) suppresses the desorption rate relative to sorption, indicating the difficulty of desorption from highly crystalline samples.

CONCLUSIONS

The predictions of the model are consistent with published experimental data as demonstrated by evaluation of the model parameters for the specific systems listed in *Table 2* and systematic comparisons between predicted and reported behaviour.

Most PET and some PC systems were classified as thick films with rapid crystallization. The data for these corroborate the predictions of diffusion controlled transport and crystallization kinetics with surface macrovoid formation. The initial negative curvature in plots of weight gain versus \sqrt{t} in thick films was also predicted, but only by numerical solution of the nonlinear equations (1). In one case, acetone in thin PC films, thin film behaviour with slow crystallization was predicted, consistent with the complete decoupling between transport and crystallization observed experimentally⁶. The remaining systems considered were associated with intermediate behaviour of the model, between the asymptotic limits. Numerical solutions simulated the experimental sorption behaviour in this region reasonably well and predicted the distinct crystallization fronts observed by Turska⁶.

The model clarifies the role of local crystallization in the transport process. During sorption, crystallization initially promotes front propagation by supplying diluent occluded from developing crystallites; the latter subsequently act as diffusive obstacles causing pseudo-Fickian transport. This interplay results in the negative curvature of the sorption curves. Furthermore, this kinetic characteristic may be accompanied, but it is not caused, by the formation of surface macrovoids.

Although *a priori*, quantitative predictions from the model are not possible, curve fitting yields phenome-

nological constants with physical meaning. For PET systems, curve fitting of weight gain data with the thick film solutions provides the diffusion coefficients for several penetrants in the swollen, amorphous component of the polymer, rather than an average over steep concentration and morphological profiles resulting from the use of Fick's law. The ratio c^*/\bar{c}^* , representing the 'partition ratio' at the moving boundary, could also be calculated. This parameter arises in formulating consistent expressions for the moving boundary velocity during sorption and desorption^{16,26,27}, where an analogy is drawn between polymer swelling and melting phenomena. Interpreting c^*/\bar{c}^* thermodynamically is probably not valid, but the constancy of the ratio in PET systems (*Table 6*) suggests that a common physical process governs the moving boundary kinetics, such as polymer yielding or microfailure.

The theory also predicts that the juxtaposition of sorption/desorption curves depends on the crystallization rate and the ultimate level of crystallinity. It appears that for penetrants inducing comparable levels of crystallinity, sorption/desorption data could be used to determine the relative crystallization rates during sorption.

ACKNOWLEDGEMENTS

The authors thank Prof L. Rebenfeld and Dr H. D. Weigmann of the Textile Research Institute for the valuable input. We gratefully acknowledge the National Science Foundation for financial support (Grant No. DMR-7905980).

REFERENCES

- 1 Durning, C. J. and Russel, W. B. *Polymer* 1985, **26**, 119
- 2 Makarewicz, P. J. and Wilkes, G. L. *J. Polym. Sci. Polym. Phys. Edn.* 1978, **16**, 1529
- 3 Makarewicz, P. J. and Wilkes, G. L. *J. Polym. Sci. Polym. Phys. Edn.* 1978, **16**, 1559
- 4 Desai, A. B. and Wilkes, G. L. *J. Polym. Sci. Symp.* 1974, **46**, 291
- 5 Titow, W. V., Braden, M., Currel, B. R. and Loneragan, R. J. *J. Appl. Polym. Sci.* 1974, **18**, 867
- 6 Turska, E. and Benecki, W. J. *J. Appl. Polym. Sci.* 1979, **23**, 3489
- 7 Ware, R., Tirtowidjojo, S. and Cohen, C. *J. Appl. Polym. Sci.* 1981, **26**, 2975
- 8 Wilkes, G. L. and Parlapiano, J. *J. Polym. Prepr.* 1976, **17**, 937
- 9 Overbergh, N., Berghmans, H. and Smets, G. *Polymer* 1975, **16**, 703
- 10 Turska, E. and Benecki, W. J. *J. Polym. Sci. Symp.* 1974, **44**, 59
- 11 Makarewicz, P. J. *PhD Thesis*, Dept. of Chem. Eng., Princeton University, Princeton, New Jersey, 1977
- 12 Lawton, E. L. and Cates, D. M. *Text. Res. J.* 1978, **48**, 478
- 13 Park, G. S. in 'Diffusion in Polymers', (Eds. J. Crank and G. S. Park), Academic Press, London, 1968, Ch. 5
- 14 Fujita, H. *Fortschr. Hoch. Polym. Forsch.* 1964, **3**, 1
- 15 Frisch, H. L. *J. Polym. Eng. Sci.* 1980, **20**, 2
- 16 Astarita, G. and Sarti, G. C. *J. Polym. Eng. Sci.* 1978, **18**, 388
- 17 Durning, C. J., Scott, M. G. and Weigmann, H. D. *J. Appl. Polym. Sci.* 1982, **27**, 3597
- 18 Sarti, G. C. *Polymer* 1979, **20**, 827
- 19 Weigmann, H. D., unpublished data
- 20 Boon, J. and Azcue, J. M. *J. Polym. Sci.* 1968, A-2 **6**, 885
- 21 von Falkai, B. and Rellensmann, W. *Die Makromol. Chemie* 1964, **75**, 112
- 22 Mandelkern, L. 'Crystallization of Polymers', McGraw Hill, NY, 1964, Ch. 8
- 23 Richtmeyer, R. D. 'Difference Methods for Initial Value Problems' V1, Interscience, NY, 1975, Ch. 6
- 24 Durning, C. J. *PhD Thesis*, Dept. of Chem. Eng., Princeton University, Princeton, New Jersey, 1983
- 25 Durning, C. J., Rebenfeld, L. and Russel, W. B., in preparation
- 26 Joshi, S. and Astarita, G. *Polymer* 1979, **20**, 1217

27 Astarita, G. and Joshi, S. *J. Memb. Sci.* 1978, **4**, 165
 28 Flory, P. J. 'Principles of Polymer Chemistry', Cornell Univ.
 Press, Ithaca, 1953
 29 Hildebrand, J. and Scott, R. L. 'The Solubility of Non-
 Electrolytes', Reinhold, NY, 1950
 30 Kelley, F. N. and Bueche, F. *J. Polym. Sci.* 1961, **50**, 549
 31 van Antwerpen, F. and van Krevelen, D. W. *J. Polym. Sci. Polym.
 Phys. Edn.* 1972, **10**, 2423
 32 Williams, M. L., Landel, R. F. and Ferry, J. D. *J. Am. Chem. Soc.*
 1955, **77**, 3701
 33 Roberts, C. *Polymer* 1969, **10**, 113
 34 Brandrup, J. and Immergut, E. H. 'Polymer Handbook', 2nd
 Edn., John Wiley, NY, 1975
 35 Sarti, G. C. and Apicella, A. *Polymer* 1980, **21**, 1031
 36 Knox, B. H., Weigmann, H. D. and Scott, M. G. *Text. Res. J.*
 1975, **45**, 203

APPENDIX

Calculation of S and h(γ)

S is defined as the maximum of the dimensionless radial growth rate of a spherulite, $G(\gamma)/G_0$, over the concentration interval experienced by the amorphous polymer, $0 < \gamma < 1$. The function $h(\gamma)$ is simply the normalized, dimensionless radial growth rate given by $G(\gamma)/SG_0$. It is an increasing function of γ for small concentrations and may go through a maximum as γ approaches 1. The calculations below are given in terms of the diluent volume fraction, $v_1 = c/\rho_s$, where ρ_s is the solvent density. The expression given by Makarewicz³ is used for G/G_0 ,

$$\frac{G}{G_0} = (1 - v_1) \exp - \left(\frac{K_1/R}{K_2 + T - T_g} \right) \exp \left(\frac{4\sigma_u \sigma_e T_m^2}{R \Delta H_u T^2 \Delta T} + \frac{2\sigma_u T_m^2 \ln(1 - v_1)}{\Delta H_u T \Delta T} \right) \quad (A-1)$$

Table A-I Physical data for solvents needed to calculate S

Solvent	Glass transition temperature* T_g (°K)	Molar volume V_1 (cm ³ /gmole)	Solubility parameter $\delta_1 \sqrt{\text{cal cm}^{-3}}$	Thermal expansion coefficient α_f (°C ⁻¹)
Methylene chloride	126.3	63.58	9.93	0.00137
Dioxane	253.0	85.2	10.0	0.00103
Acetone	128.4	73.43	9.77	0.00143
Nitro-methane	194.4	53.96	12.7	0.0012†

* Estimated as 50°C below freezing point

† Typical value for liquids

Data were compiled from the CRC Handbook (46th edn.), Lange's Handbook (12th Edn.) and the references cited in the Appendix

Table A-II Physical data for polymers needed to calculate S

Symbol	Definition	PET	Values PC	IPS
K_1/R (K)	WLF constant	777	2080*	2080
K_2 (K)	WLF constant	24	51.6*	75
$4\sigma_u \sigma_e$	see Ref. 3	513	513†	279
$R \Delta H_u$				
$2\sigma_u$	see Ref. 3	0.26	0.26†	0.2
ΔH_u				
T_m^0 (K)	Polymer melting point	546	538	513
ΔH_u (cal/gmole)	Polymer heat of fusion	29	26.8	19.3
V_2 (cm ³ /gmole)	Polymer specific volume	0.75	0.83	0.95
δ_2 (cal cm ⁻³) ^{1/2}	Polymer solubility parameter	9.8, 12.1	9.5	9.1
T_g^0 (K)	Glass transition temperature	343	422	358
α_f^0 (K ⁻¹)	Change in polymer thermal expansion coefficient at T_g	2.1×10^{-4}	3.8×10^{-4}	3.7×10^{-4}

* Universal constants

† Assumed to be the same as in PET

Data were compiled from the references cited in the Appendix

The diluent affects the value of the melting point and the glass transition temperature through the relationships

$$\frac{1}{T_m} - \frac{1}{T_m^0} = \frac{R \bar{V}_2}{\Delta H_u V_1} (v_1 - \chi v_1^2) \quad (A-2)$$

from Flory's melting point theory²⁸,

$$\chi = \chi_s + \frac{\bar{V}_1}{RT} (\delta_1 - \delta_2)^2 \quad (A-3)$$

from the regular solution theory²⁹, and

$$T_g = \frac{T_g^0 + v_1 [(\alpha_f^s/\alpha_f^0) T_g^s - T_g^0]}{1 + v_1 [(\alpha_f^s/\alpha_f^0) - 1]} \quad (A-4)$$

from the free volume theory of Kelley and Bueche³⁰. The symbols in (A-1)–(A-4) and their values compiled from the literature^{3,7,9,20,31–36}, are summarized in Tables A-I and A-II. The nomenclature is identical to that in Ref. 3. The value of χ_s is taken as 0.35. Following Knox *et al.*³⁶ the solubility parameter for PET was taken as 9.8 or 12.1 cal cm⁻³)^{1/2}, depending on the solvent, to give a minimum value of the quantity $(\delta_1 - \delta_2)^2$. To calculate S, the maximum value of G/G_0 is found with the upper bound on the volume fraction diluent given in Table 2 of Ref. 1. Given S, $h(\gamma)$ follows from its definition.